Remotely Operated Vehicle for a continental shelf research

Eng. Konstantin Chterev MSc.

High education code 4: „Natural science, Mathematics and computer science".
Professional area code 4.4: „Earth science"
Doctoral programme „Oceanology".

Summary of a doctoral thesis for the degree of
"Philosophiae Doctor"

doctoral advisor: Assoc. Prof. Dimitar Petkov Dimitrov PhD

Varna   December 2019

Abstract

This thesis is about the overall architecture and the main components of an observational class Remotely Operated Vehicle (ROV). The research has focused on modelling the ROV as a distributed network system, control protocols and data transfer. In addition, based on the theoretical research, a working ROV has been designed, built, tested and used in several research projects in the Black Sea region.

Currently, ROVs are very popular and intrinsic part of any underwater activities. Numerous academic institutions even have departments, dedicated to do underwater vehicle research. Despite that, the author could not find many articles on the overall ROV design, component interconnection and networking. Most of the papers are related to navigation, autopilots, hydrodynamics, stability, trajectory tracking and terrain following. Few papers address the overall design, but the theory in them is out of context and sketchy.

This thesis fills the gap in the research in various areas. First, it introduces a concept of a ROV, based on the 7 layer OSI model. The model takes into account only the minimum required components - ROV control console (RCC), tether, thrusters and camera, but any other auxiliary equipment could be easily included. Second, a new protocol for minimising the control lag is introduced and a new method for the video stream transfer is implemented. The model is analysed for bandwidth and verified measuring the real network traffic in the built ROV. Third, a ROV system power supply is designed and created. It is analysed for stability and tested in the real operation. Fourth, the thruster system is created and optimised for the specific needs of the ROV. The thrusters are designed, built and tested for efficiency. Fifth, the camera-lights system is analysed for optimum colour temperature. The most suitable LEDs for ROV use are found.

The performance of all components in the scope is measured and recorded. Finally the overall ROV behaviour, as observed in the field test, is analysed. The methodology and the results are presented in the relevant sections.

Абстракт

Този дисертационен труд е относно цялостната архитектура и основните компоненти на система Подводен Апарат с Дистанционно управление (ПАДУ). Изследването е фокусирано върху подсистемите за захране, задвижване и комуникации. Изследван е също модел на ПАДУ като дистрибутирана информационна мрежа, с иновативен команден протокол. ПАДУ система е изработена използвайки резултатите от теоретичното изследване и реално изполвана в няколко проекта в акваторията на Черно Море.

Понастоящем ПАДУ са много популярни и съществена част от каквито и да е подводни изследвания. Много академични институции имат секции, занимаващи се изключително с изследвания на подводни апарати. Въпреки това, наличните статии по цялостни ПАДУ система дизайн и комунккации между подсистемите и са много малко. Повечето публикации са за навигация, хидродинамични характеристики, стабилност и автопилоти. Няколко публикации засягат цялостния дизайн, но теорията в тях е повърхностна и непълна.

Този труд запълва тази празнина в няколко области на изследванията. Първо, предложена е мрежова концепция на ПАДУ, базирана на 7 слойния OSI модел. Моделът включва минималната конфигурация от компоненти - Конзола за Дистанционно Управление (КДУ), тетер, тръстери и камера, като всяко допълнително устройсво може да бъде добавено към модела. Второ, иновативен протокол е създаден с цел минимизиране на закъснението в синхронизация между отделните компоненти. Моделът е изследван за изисквания към пропусквателна способност на мрежовите канали и проверен на практика с реално работеща ПАДУ система. Трето, създаден е модел на захранването на ПАДУ, което се оказва нетривиален проблем. То е изследвано за стабилност, изработено и тествано в лабораторен и реален проект. Четвърто, системата за задвижване е изледвана и оптимизирана за конкретните цели на ПАДУ. Тръстерите са проектирани, изработени и тествани за ефективност. Пето, систетмата от видеокамера и светлини е анализирана и изследвана за оптималност, намерени са LED светлините с най-походяща цветова температура за подводни апарати.

Ефективността на отделните компоненти е измерена и записана. Поведението на цялата ПАДУ система е наблюдавана в реален екперимент и анализирана. Методологоята на изследванията е дадена в съответните секции.

Chapter 1:   Introduction

1.1   Definitions

ROV - Remotely Operated Vehicle, is an unmanned submersible, controlled via cable - tether, allowing the operator to work in a safe environment, while the apparatus executes various underwater tasks.

Tether - a reinforced cable, which carries power, data and control signals between the ROV and the RCC.

ROV Control Console (RCC) - ruggedized computer module with various interfaces, allowing the operator to control the ROV motion and accessories, as well as visualise and record the received telemetry and video data.

A ROV System comprises of a Remotely Operated Vehicle, tether and RCC. This is the minimum set of components making a ROV operational.

1.2   Requirements

- Product capabilities - Black Sea continental shelf research

- Cost - half of similar commercial ROVs

- Time - 2-3 years

As a commercial reference is chosen the Seaeye Falcon made by SAAB. All the requirements are set to be equal ot better than Seaeye's with a budget less than a half of it's price - Table 1.1.

Table 1.1 Seaeye Falcon to Sea Turtle II comparison

Parameter	Seaeye	Sea Turtle II
Dept rating [m]	300	300
Tether length [m]	450	550
Motors	DC Brushless	DC Brushless
Thrusters	4 x horisontal, 1 x vertical	4 x horisontal, 4 x vertical
Max. bollard thrust [kgf]	50	50
Controll system	Distributed	Distributed
Camera	Colour 480 TVL	Colour HD 720p/1080p
Lights [lm]	6400	8000
Navigation	Compass, gyro, depth	Compass, gyro, depth
Power	220/240V 2.8 kW	220/240V 2.4 kW
Budget	50,000.00 USD	20,000.00 USD

1.3   Problem outline

The ROV is a complex apparatus and building one is an interdisciplinary problem. Deep knowledge in the fields of Physics, Chemistry, Electronics, Communications, Mechanical and Electrical engineering is required. Often, the financial viability is the driving force behind the R&D in the commercial companies. Thus, many ROV components are either underdeveloped or left unchanged for decades. This thesis attempts to address all these issues and to propose the best available technology for all major ROV components, keeping in mind the budget limitations. Several contributions are made, bringing together knowledge from various fields in the science in creating a novel ROV which has no analogue in the commercial market. More about the problem outline is given in the relevant chapters.

1.4   Goals and objectives

The main goal of the research is creating a ROV system architecture which can be used as a platform for building a ROV suitable for Black Sea shelf exploration. The second goal is actually building such apparatus and testing it in a real life research. These goals lead to the following objectives:

- Research the existing ROV state of the art

- Create a requirement list for the project

- Split the ROV system into a manageable subsystems

- Create the overall system architecture

- Design, manufacture and test all the subsystem

- Test and review the results of the whole ROV system

1.5 Contributions

1. Chapter 2. A power model of a ROV system is created. An equation for power transfer is devised.

2. Chapter 2. Transfer function of a distributed power supply system is derived. The system is analysed and verified for stability.

3. Chapter 3. A network model of a ROV is created. A novel communication protocol is developed in order to reduce components and increase reliability.

4. Chapter 4. A tether, based on a Power Twisted Pair (PTP) network channel using Frequency Division Multiplexing (FDM) is developed and analysed.

5. Chapter 5. Novel motor control algorithm is designed and implemented.

6. Chapter 5. Dedicated ROV propeller is designed, suitable for the high K_v brushless DC motors.

7. Chapter 6. Various LED lights are analysed for performance in water. The most suitable colour temperature is found.

8. Chapter 7. IP camera is tested for lag and performance. Bandwidth requirements are devised.

9. Chapter 8. A ROV system is built, based on the theoretical research. The system is tested in year 2016 on board RV Akademik in the Black Sea.

Chapter 2:   Power

Based on simplicity and cost, a decision was made for the power source to be the European domestic mains standard Schuko - 220V AC, 50Hz, 16A. The maximum available power at the source in this case is around 3.5kW. From this available power and the tether power wires construction, the power available to the ROV can be derived.

2.1   The long wire problem

Regarding power, one of the major differences between a ROV system and other electrical appliances is the much longer power cord (tether). Transferring power over a long distance is not a trivial exercise. Often, the cable resistance is comparable to the resistance of the load. The derived equation for the cable resistance is:

$$R_w \approx \frac{3.3 \times 10^{-2} l}{A[\text{mm}^2]} \tag{2.1}$$

Here, R_w is the total resistance, l is the cable length and A is the wire cross section in mm^2. The high cable resistance leads to a power transfer issue, which is analysed using the maximum power transfer theorem, which states that the maximum power is transferred when the cable and the resistances are the same. From the theorem and Equation 2.1, the power maximum power transfer equation is derived:

$$P_{max} \approx 7.62 \frac{A U_{in}^2}{l} \tag{2.2}$$

Where P_{max} is tha maximum possible transferred power and U_{in} is the voltage of the vessel power source. The equation 2.2 is extremely useful in both designing a new apparatus or maintaining a system with various optional tethers. The three independent variables A, U_{in} and l can be chosen to achieve the desired ROV operational range and speed. The inevitable outcome of the high cable resistance is a significant voltage drop over the thether, which is exactly half of the U_{in} in a maximum power transfer. This must be taken into account in the power supply (PSU) design.

2.2   The PSU

The ROV PSU must either work in a wide input range of voltages, ot a voltage drop compesation must be implemented. The later is being attempted in the thesis.

2.2.1   Voltage grop compensation

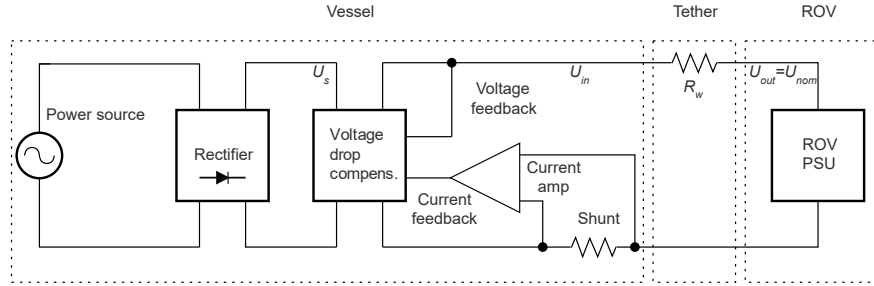The following figure shows the voltage drop compensated power model - Fig. 2.1.

Fig. 2.1 Sea Turtle II power model.

It is decided a standard off-the-shelf commercial PSU to be used in the ROV. The voltage drop component though is not a standard equipment and has to be designed. Targeting $U_s = 2U_{nom}$, a preliminary stage is needed which steps-up twice the mains voltage. This is easily done by a step-up mains transformer.
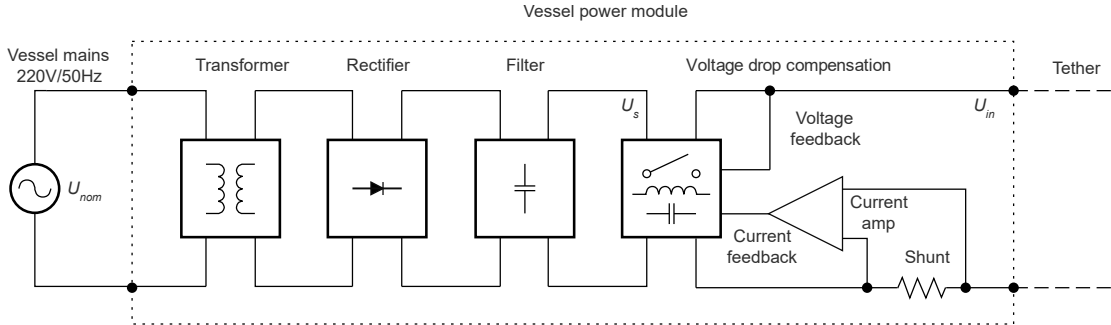
Fig. 2.2 Vessel power module.

The vessel part of the power system is presented in Fig. 2.2. All component are standard apart from the voltage drop compensation unit. In general, this is a DC/DC converter with the output characteristic depending on the output current. The derived Equation 2.3 gives the required vessel PSU voltage.

$$U_s = \frac{R_w P_r}{U_{nom}} + U_{nom} \tag{2.3}$$

2.2.2 Power supply system DC analysis

The DC analysis is fairly strait forward. C_{rov} can be ignored for DC, so only 2 resistors in series remain-
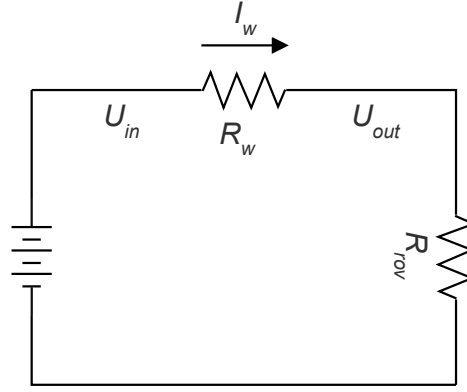

Fig. 2.3 DC equivalent circuit.

At minimum power $R_{rov} \approx \infty$, so $I_w \approx 0$ and $U_{out} \approx U_{in}$. At maximum power $R_w \approx R_{rov}$. So $I_w \approx U_{in}/2R_w$ and $U_{out} \approx U_{in}/2$. The load R_{rov} DC model is

$$R_{rov} = \frac{P}{I^2} = \frac{U_{out}^2}{P} \tag{2.4}$$

2.2.3 Power supply system AC analysis

The main purpose of the AC analysis is verifying the system stability. The AC equivalent circuit in the **S** domain is
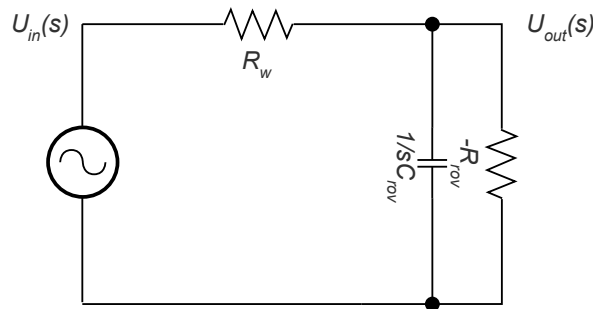

Fig. 2.4 AC equivalent circuit.

With a transfer function:

$$G(s) = \frac{\frac{1}{R_w C_{rov}}}{s + \frac{1}{R_w C_{rov}}\left(1 - \frac{R_w}{R_{rov}}\right)} \tag{2.5}$$

The system is stable when the poles (the denominator roots) lay on the left hand plane of the pole-zero plot, i.e. the poles must be negative. This condition is satisfied when

$$\frac{R_w}{R_{rov}} < 1 \qquad (2.6)$$

From the power transfer theorem this condition is always satisfied, so the PSU is stable.

Chapter 3:   Communications

The ultimate purpose of any inspection class ROV is the ability to be located in a particular underwater point, providing video, telemetry and other sensory data to the operator on the surface. Transferring meaningful information (referred usually as "data") from one point to another is called "communication", which is the subject of this chapter.

Two data stream need to be supported - a high bandwidth video and a low bandwidth command and telemetry. It makes sense to split these streams in two separate networks as the requirements are completely different. The resulting topology is shown on Fig. 3.1.
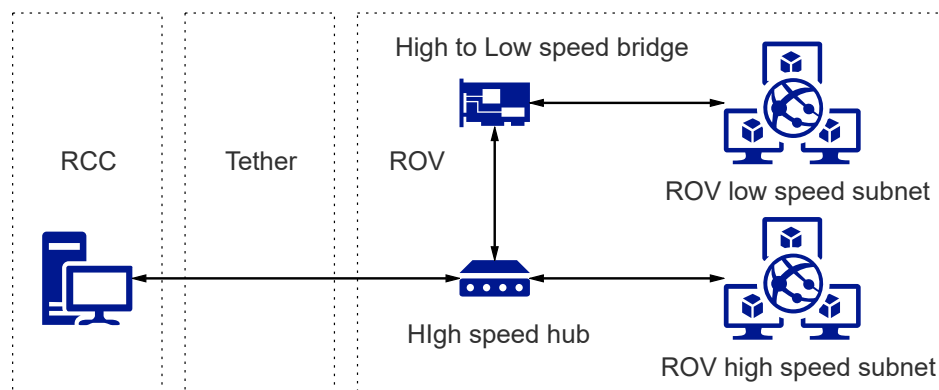

Fig. 3.1 High performance network with a low speed subnet.

The low speed network is designed loosely based on the industry LIN standard, with an improved functionality for underwater applications. A novel data link protokol is developed as well. The final architecture is called LUNA - Lightweight underwater network architecture. LUNA has several advantages over the trivial networks for ROV use:

- High flexibility

- Parallel high speed and low speed networks

- Low cost

- Low wire count

- Low connector pins count

- Easy adding new nodes

- Easy programming

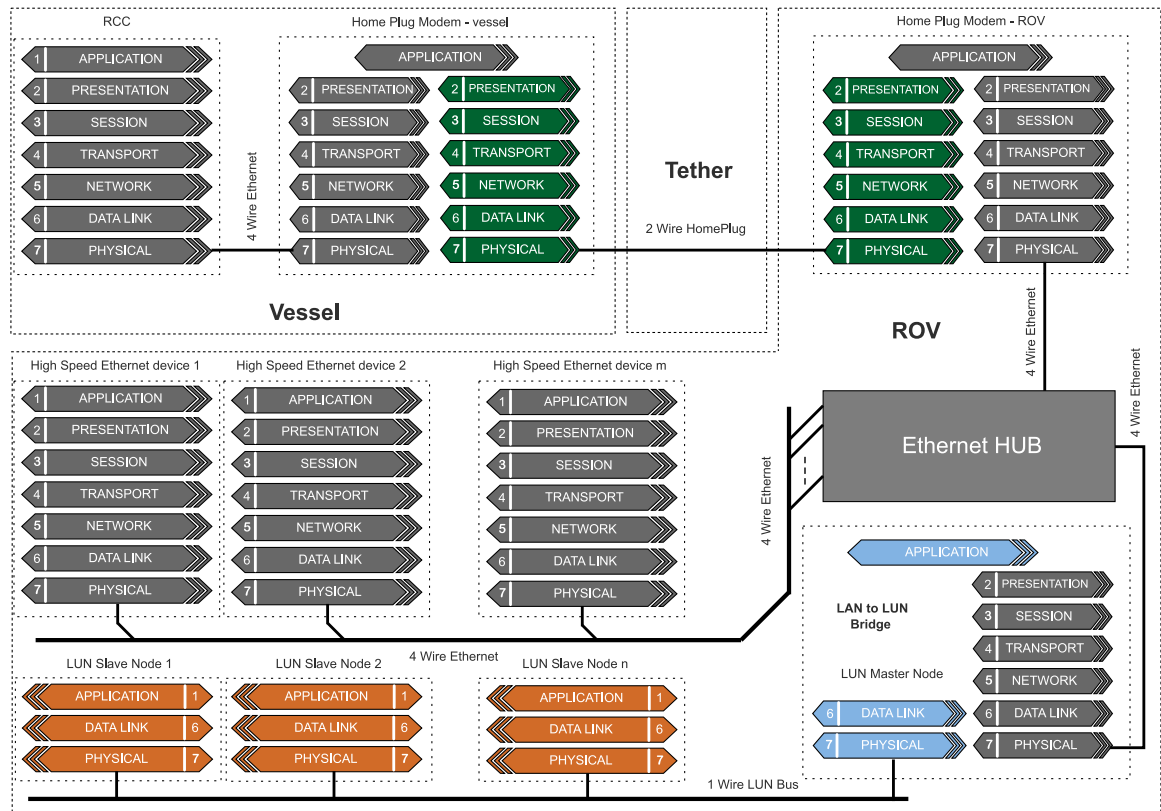- Ability to use off-the-shelf hardware components

Fig. 3.2 LUNA OSI model.

Chapter 4:   Tether

A tether is the cable connecting the ROV with the RCC. In order to achieve the desired functionality, the tether must contain the following:

- Power wires

- Communication wires/optical fibre

- Reinforcing threads

- Buoyancy correction filler

- Protective outer jacket

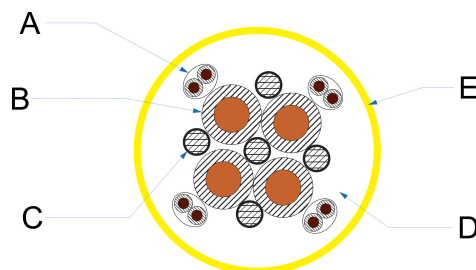A cross section of SAAB Falcon Seaeye tether is presented on Fig. 4.1.

Fig. 4.1 SeaEye Falcon tether cross section.

- A - 4x screened communication twisted pair wires

- B - 4x Power wires

- C - Vectran reinforcing members

- D - Poly-foam

- E - High abrasion resistance outer jacket

The tethers vary in the number of wires, cross section etc. but more or lees they follow the template on the Fig. 4.1.

4.1   Physical connection

As being always physically present, the tether impacts the whole system in several ways:

- Buoyancy. The tether buoyancy is controlled by the D member, which cross section must comply with the following equation in order the tether to be neutrally buoyant - Equation 4.1

$$S_D(1 - SG_D) = S_A(SG_A - 1) + S_B(SG_B - 1) + S_C(SG_C - 1) + S_E(SG_E - 1) \qquad (4.1)$$

  Where $SG_A, SG_B, SG_C, SG_D, SG_E$ are the specific gravities of the tether members from Fig. 4.1 and S_A, S_B, S_C, S_D, S_E are their cross sections.

- Strength. In most ROV systems the tether is the only physical connection to the vessel. This means that the deploying relies on the strength of the tether as a safety link. If the breaking strength is not big enough, the tether could snap and the ROV can be lost. The strength equation for the C member is Equation 4.2

$$A_r[\text{mm}]^2 \approx \frac{10 k_s W_{ROV}[\text{kg}]}{\sigma[\text{Mpa}]} \qquad (4.2)$$

- Drag. This is one of the most unpleasant features of the tether. The ROV must pull the tether behind all the time, while part of the power is lost in the consequent drag. This physical property of the tether often limits the maximum deploying depth due to the available power being less than required for overcoming the tether drag force. The research on the tether drag is of a little practical use, so the general rule of the thumb is thiner tether and more power, when the drag is an issue.

4.2   Power and Communications

The Equation 2.2 defines the required power wires cross section, depending on the total power and tether length. The wires insulation thickness and material is defined by the maximum voltage U_s. Knowing the cross section and the insulation makes possible a cable selection from a standard of-the-shelf products. For instance, the example in Section 2.2 defines the power wire with $A = 2.5\text{mm}^2$ and $U_s = 338.5\text{V}$. A cable is chosen with $A = 2.5\text{mm}^2$ and $U_s = 600\text{V}$ - the datasheet is given in Appendix **??**. The idea is to make this cable a twisted pair, so it can be used for communication too. The resulting PTP is shown on Fig. 4.2:

The most important parameter of any transmission line is the characteristic impedance Z_0 which depends on the material properties and geometry of the line. Z_0 has a practical importance. The transmission line must be terminated by an active resistor with the same value, so the line can have no reflections and the signal quality is not affected - Fig. 4.3.
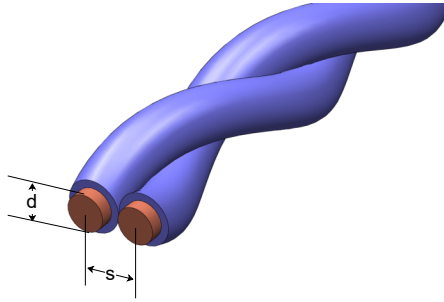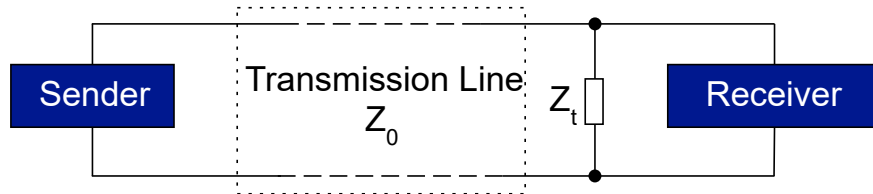
Fig. 4.2 Power Twisted Pair cable.

Fig. 4.3 Transmission line termination.

It is not important what the exact value of Z_0 is, as long as it is known, so that the termination resistance $Z_t = Z_0$. The UTP characteristic impedance is:

$$Z_0 = \frac{120}{\sqrt{\epsilon_r}} \ln \frac{2s}{d} \tag{4.3}$$

Where ϵ_r is the dielectric constant of the insulator, s is the distance between the wires and d is the wire diameter (Fig. 4.2). For the cable in the exaple above: From the selected wire datasheet - $d = 2$mm, $s = 3.6$mm and $\epsilon_r = 5$. The characteristic impedance is:

$$Z_0 = \frac{120}{\sqrt{5}} \ln \frac{2 \times 3.6}{2}$$

$$Z_0 \approx 70\Omega$$

Using the same wire pair for power and communication makes the tather extremely easy to make and repair. There are just two wires in a PTP configuration, plus the usual and unavoidable reinforcing members and the buoyancy foam - Fig. 4.4.

- A - Reinforcing members

- B - Outer jacket
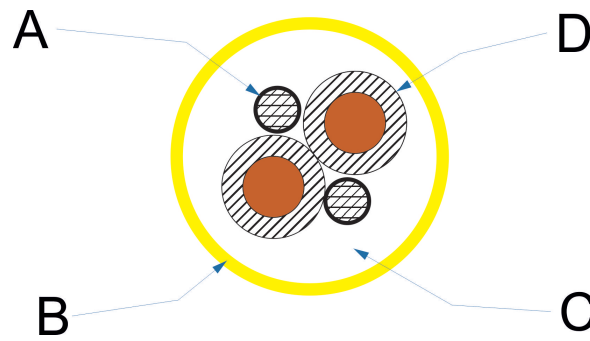
- C - Poly-foam

- D - PTP

Fig. 4.4 Cross section of PTP tether.

The design of the real tether used with Sea Turtle II is given in Chapter **??**.

Chapter 5:   Thruster

The device, converting electricity into force - thrust is called thruster and acts like rocket engine, jetting out water, moving the vehicle in the process Fig. 5.1.
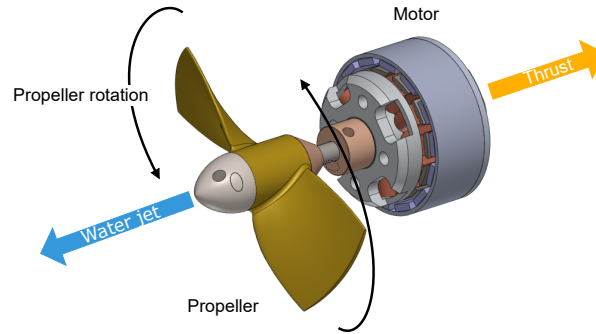

Fig. 5.1 Electric motor and propeller thruster.

A thruster consists of a motor, a propeller and an Electronic Speed Controller - ESC, in order to make the thrust controllable by the ROV operator.

5.1   Motor

A Brushless DC (BLDC) motor is chosen for the project. As the name suggest, there are no commutation brushes, so the motor requires ESC - electronic speed controller to in order to run. The motor is characterised by a speed constant K_v which is the ideal motor RPM output e per volt of supplied voltage. The process of motor selection is called motor sizing and it is based on 2 factors:

- **Required Power.**

$$V_m = C_V \ \frac{P_N}{f B_r H_c} \tag{5.1}$$

  Here, V_m is the total volume of the magnets, P_N is the maximum rated output power, B_r is the residual magnetic flux density, H_c is the magnets coercive force, F is the rotation frequency and

C_V is a coefficient between 0.54 and 3.1. All members on the right are known for certain motor, so V_m can be calculated. In practice, the problem is solved in reverse - having particular off-the-shelf motor, the correct output power P_N is calculated and checked if it fits the requirements.

- **Required Speed.** The current through the motor should be kept to minimum to minimise the resistive losses in the cables and windings. For certain power, the supplied voltage should be as high as possible, so a motor with the lowest K_v should be selected.

5.2 Electronic Speed Controller - ESC

The ESC is an electronic circuit, which accepts a set point - the motor speed - and converts it to a sequence of commutation, needed to run the BLDC with the required speed. All the ESCs have as a minimum two major blocks - power and control - Fig. 5.2.
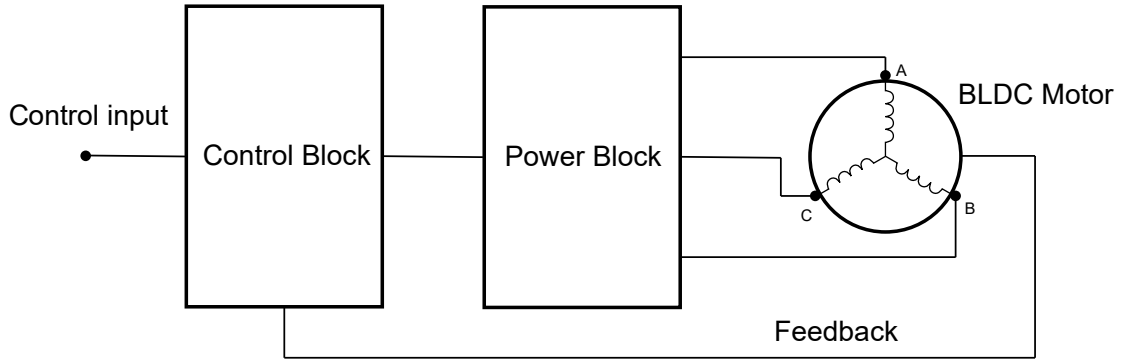

Fig. 5.2 ESC block diagram.

The power block is a three phase Pulse Width Modulation (PWM) controlled bridge, also called three phase inverter - Fig. 5.3.
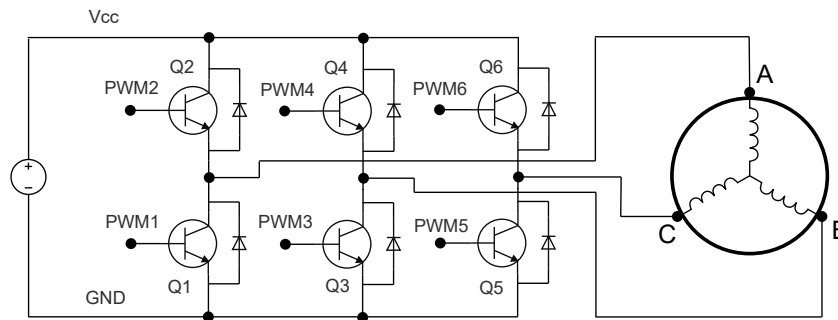

Fig. 5.3 ESC three phase inverter.

The control block - Fig. 5.4 - serves, as a minimum, three main purposes -

- Accept some input for the desired speed and direction. This parameter is called motor Set Point (SP).

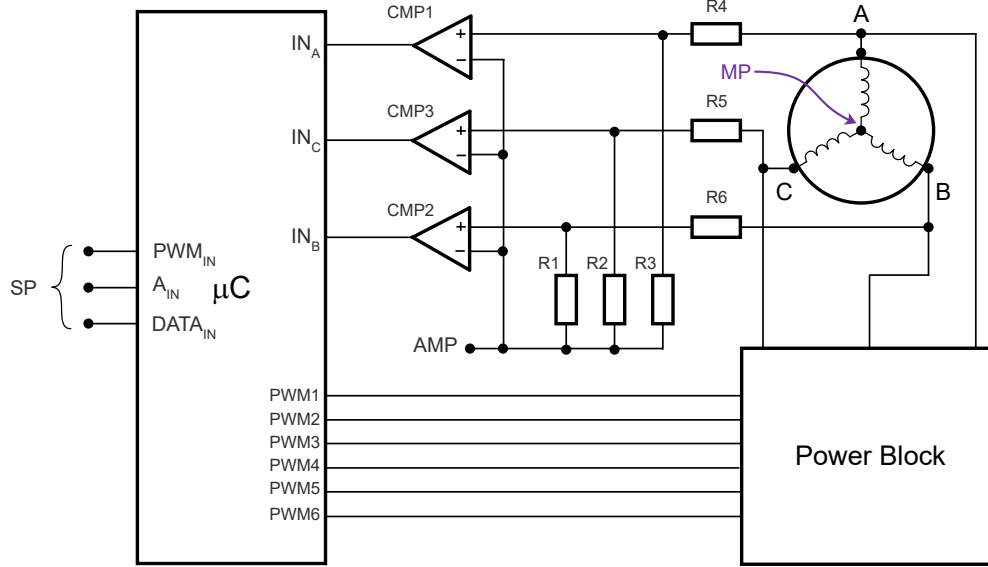- Accept the feedback from the motor rotation.

- Generate the desired PWMs.

Fig. 5.4 ESC control block.

5.2.1 ESC control algorithm

The FPZC algorithm depends on BEMF (Back Electromotive Force), i.e. it works only when the rotor is turning and generating BEMFs. In normal operation, only 2 phases are energised, when the third one is left to float. The ESC monitors the floating phase and detects when it reaches the AMP-artificial mid pint of the power supply voltage. The commutation time depends on this zero cross detection time. The best way to describe the algorithm is by reviewing the states and state change conditions. The application starts with the default state STOP.

- **STOP**. In this state the algorithm forces the motor to stop rotating. This is achieved by electrical breaking.

- **STAND BY**. In this state the ESC still applies some PWM to the phases in order to keep the rotor in a steady, non-rotating state. The exit condition of this state is SP $<>$ 0 when the state is changed to ALIGN.

- **ALIGN**. In this state, the ESC switches chosen phases, so that the rotor is aligned to a know position.

- **RAMP**. In this state the algorithm attempts to start the motor. This is done by switching the phases according to 6-step control sequence.

- **RUN**. In RUN state, the algorithm performs phase locked loop PLL control, which keeps the motor running over a maximum operation point range. The principle is illustrated on Fig. 5.6.
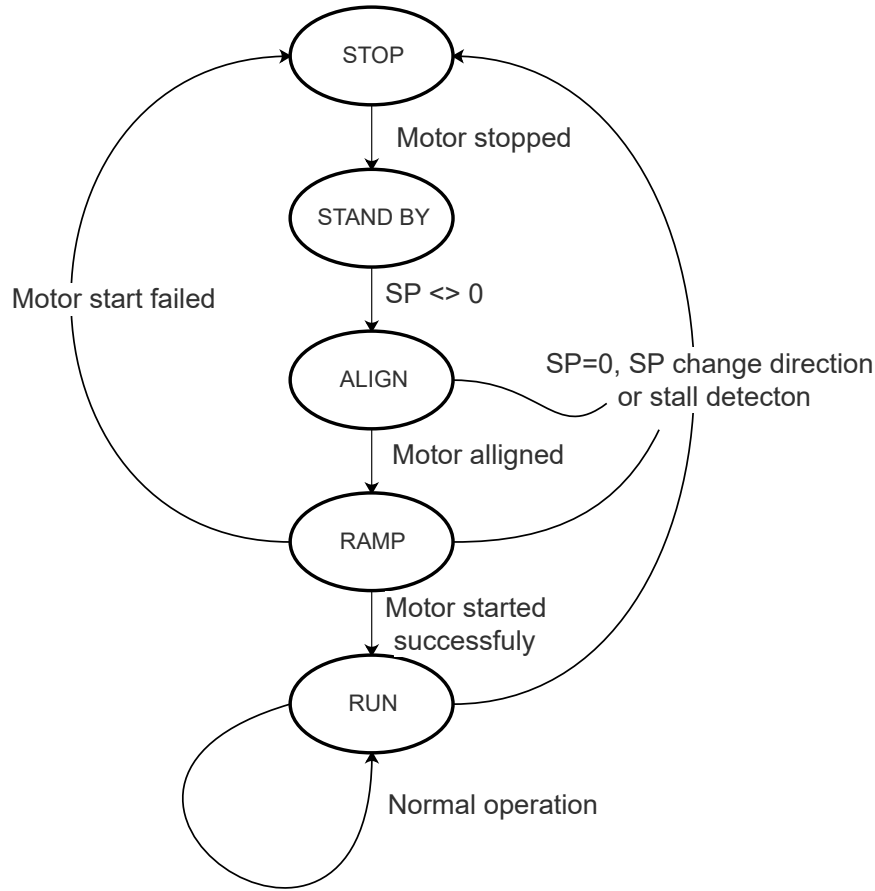
Fig. 5.5 ESC control algorithm.

5.2.2   FPZC method and stall detection

Fig. 5.6 depicts idealised zero-crossing detection. In practice, the BEMF waveform is more complicated - Fig. 5.7.

The inductive kickback creates a major problem to the FPZC method. It generates at least two zero crossing events, which must be ignored by the algorithm. As the events are very close to the commutation, a blanking time T_b is used to prevent these false zero crossings to be considered. The algorithm must ignore all the events arriving at $t < T_b$. T_b is a configurable parameter and depends on the motor construction. Usually, motors with lower K_v have larger inductance phases, hence larger T_b is required. The side effect of the blanking time is the maximum speed at which the FPZC method can operate. The maximum mechanical frequency ω_{mmax} is

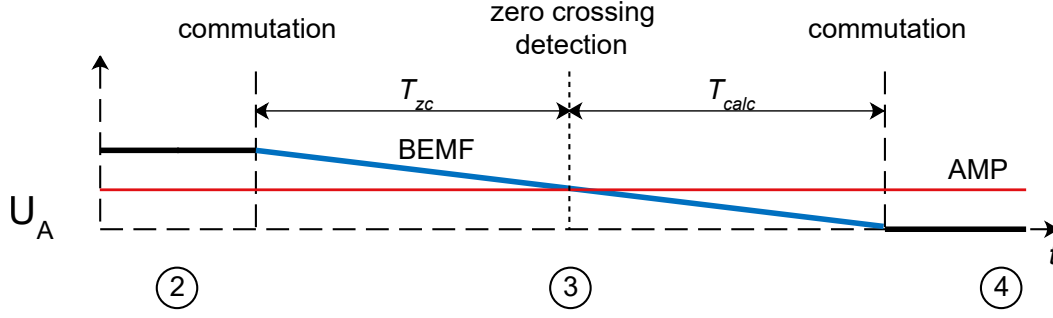$$\omega_{mmax} = \frac{1}{6p2T_b} \tag{5.2}$$
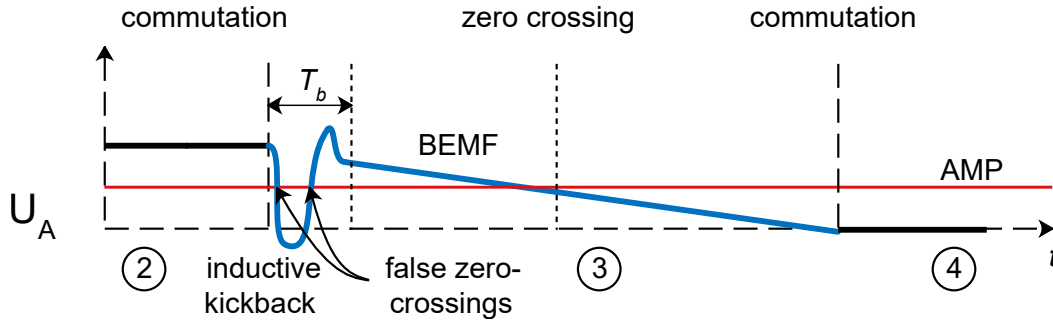
Fig. 5.6 Zero crossing PLL.

Fig. 5.7 Real BEMF with inductive kickback.

where p is the number of motor pole pairs. One of the problems with the sensorless control methods is the difficulty of detecting the motor stall state. Usually the published algorithms work in a time domain. Due to the motor inertia, the expected zero crossing event can be predicted. If the event does not happen in a certain time interval, the motor is considered stalled. This methods suffer from several drawbacks and it is much easier, to work in the frequency domain instead of the time domain. The ESC simply checks if the motor measured frequency is close to the theoretical maximum. If yes, the motor is at stall - Equation 5.3:

$$\omega_m > \omega_{mmax} - D_f \tag{5.3}$$

D_f is a configurable parameter giving the margin of the detection.

5.3   Propeller

The propeller is defined mainly by the blade geometry, the number of blades and the pitch. Historically, the blade geometry is given in tables, where the contour of the 2D expanded section is given as a percentage of the thickness vs. the maximum blade thickness. The rows of the table give the section position, usually by r/R. The columns present the distance of the thickness from the leading edge.

The cell value is so called ordinates, which are the relative thicknes at this r and distance. Table 5.1 illustrates such approach.

Table 5.1 Blade thickness table.

	Distance of the ordinates from the maximum thickness											
	From maximum thickness to trailing edge					From maximum thickness to leading edge						
r/R	100%	80%	60%	40%	20%	20%	40%	60%	80%	90%	95%	100%
						Back						
0.2		38.23	63.65	82.4	95	97.92	90.83	77.19	55	38.75	27.4	
0.3		39.05	66.63	84.14	95.86	97.63	90.06	75.62	53.02	37.87	27.57	
0.4		40.56	66.94	85.69	96.25	97.22	88.89	73.61	50	34.72	25.83	
0.5		41.77	68.59	86.42	96.6	96.77	87.1	70.46	45.84	30.22	22.24	
0.6		43.58	68.26	85.89	96.47	96.47	85.89	68.26	43.58	28.59	20.44	
0.7		45.31	69.24	86.33	96.58	96.58	86.33	69.24	45.31	30.79	22.88	
0.8		48.16	70.84	87.04	96.76	96.76	87.04	70.84	48.16	34.39	26.9	
0.9		51.75	72.94	88.09	97.17	97.17	88.09	72.94	51.75	38.87	31.87	
1		52	73	88	97	97	88	73	52	39.25	32.31	
						Face						
0.2	20.21	7.29	1.77	0.1		0.21	1.46	4.37	10.52	16.04	20.62	33.33
0.3	13.85	4.62	1.07			0.12	0.83	2.72	6.15	8.28	10.3	21.18
0.4	9.17	2.36	0.56				0.42	1.39	2.92	3.89	4.44	13.47
0.5	6.62	0.68	0.17				0.17	0.51	1.02	1.36	1.53	7.81

Here the distances are given from te point of maximum thickness to both leading and trailing edges. The values in the table are relative. This means that from them any size blade could be constructed. Similar table defines the section chord length, again vs. r/R ratio. The only parameter that cannot be derived from such tables is the propeller **pitch**. Propeller pitch is the distance the blades travel through the water per revolution, as if the water was a solid body Fig. 5.8.
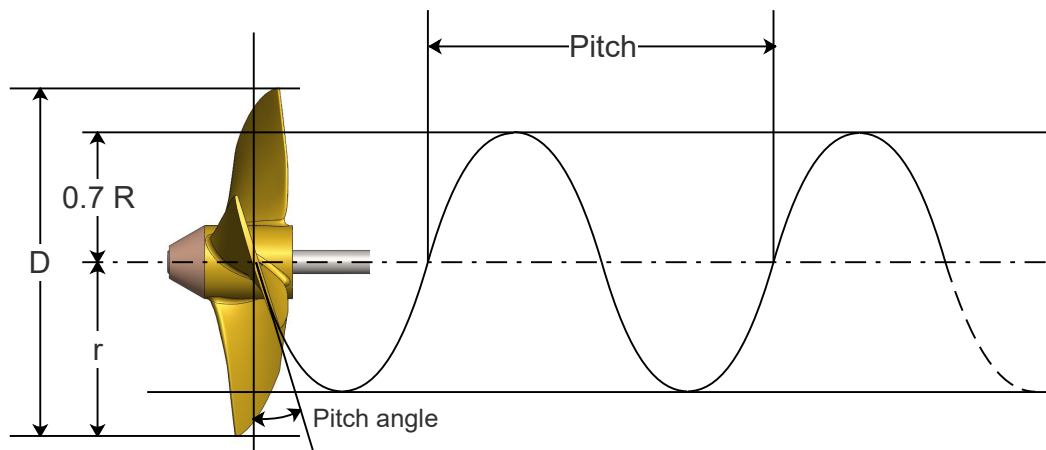

Fig. 5.8 Propeller pitch.

This distance obviously depends on the angle between the BCS chord and the plane of rotation, called **pitch angle**. The pitch angle varies from root to tip. This is due to the different axial speeds at different r which must be compensated in order to achieve equal pressure and less stress along the blade length. As the pitch varies, it is accepted that the propeller pitch is the pitch at $r = 0.7R$. Pitch has an unit of length and obviously depends on the propeller size. In order to make this property unit-less, the **pitch ratio** is used. Pitch ratio Pr is the pitch divided by the propeller diameter

- $P_r = Pitch/D$. This way, from an unit-less table values and P_r, a propeller construction can be derived in any size.

5.3.1 Propeller selection

The ultimate purpose of the propeller design is to fit particular project requirements. As a general requirement, the propeller must be inexpensive, easy to manufacture, efficient across the thruster operating point and suitable as size. Most of these requirements are mutually exclusive and a good compromise must be made. A good start with the design is selection of a close match from a standard series and then workout the best modification if necessary. Starting from the classification points -

- **Number of blades**. Theoretically, the most efficient propeller has 2 blades. For a ROV, there are no other requirements like noise reduction, so the choice is to go with 2 blade propeller.

- **Pitch**. The variable pitch propellers are far too expensive, so fixed pitch propeller is used.

- **Duct**. As mentioned, all ROVs have ducted propellers, so ducted propeller is used for this project. The duct itself can be chosen from a selection of series too.

- **Series**. The most popular ducted propeller series are Kaplan (or Ka) series. A Ka propeller is used for the project.

In summary, two bladed, fixed pitch Kaplan ducted propeller is produced and tested. The performance experiments are conducted and discussed in Chapter 8.

Chapter 6:   Lights

LED lamps are chosen for the project and the power and the colour must be selected in order to fit the requirements.

6.1   Power

There are two aspects the of a light source power ratings. One is the electrical power consumed by the device, given in **watts**. The other, more suitable parameter is called **lumen** and it is linked to the light intensity or lamp brightness. The stated rating in lumens defines the total light quantity of visible light emitted by a light source. For practical purposes, the most important parameter is not the actual lamp brightness, but the amount of light transferred to an object at certain distance. This is covered by the unit of illuminance - **lux** lx, which is nothing more but the lumens delivered per certain area -

$$1lx = 1lm/m^2 = 1cd.sr/m^2 \tag{6.1}$$

For observation purposes by a video camera, the lux is the most important parameter. Most cameras sensitivity is given in luxes and require illuminance of around 100 lux to operate. Also, the camera has defined point of view, measured in vertical and horizontal **angles of view** or **field of view**. This information, together with the chosen distance of view at about 3m is enough to be able to calculate the required lights power rating. Fig. 6.1 shows simplified light - camera setup.

The derived equation for the LED intensity is:

$$L_{lm} = C_{lx}\pi d^2(\tan v + \tan h) \tag{6.2}$$

where C_{lx} is the illuminance required by the camera. The Equation 6.2 is valid when the media is completely transparent and not absorbing the emitted light.
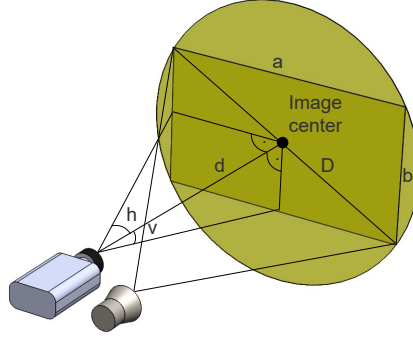
Fig. 6.1 LED lamp and camera setup.

6.1.1 Colour

The light loss due to absorption is defined by a coefficient $\alpha(\lambda)$, due to scattering by $\beta(\lambda)$. The total attenuation is defined by $c(\lambda) = \alpha(\lambda) + \beta(\lambda)$. The light loss is exponential with the distance d and covered by the following law:

$$L_{lm}(d) = L_{lm}(0)e^{-c(\lambda)d} \tag{6.3}$$

$L_{lm}(d)$ is the transmitted intensity of the light light, $L_{lm}(0)$ is the incident intensity. $c(\lambda)$ for for pure water is given in a plot - Fig. 6.2.
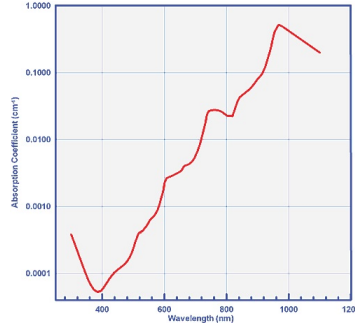
Fig. 6.2 Pure water absorption coefficient $\alpha(\lambda)$.

The final equation for light power becomes:

$$L_{lm}(0) = C_{lx}\pi d^2(\tan v + \tan h)e^{\alpha(\lambda)d} \tag{6.4}$$

In order to estimate the required light source lumens, the parameters needed are:

- d - required operational distance to the object of interest.

- v, h - camera vertical and horizontal half angles.

- C_{lx} - illuminance required by the camera.

- $\alpha(\lambda)$ - absorption coefficient, obtained from the graph on the Fig. 6.2 and

- λ of the chosen light source.

6.1.2   LED selection

The LED colours are defined as **colour temperature**. The colour temperature is the temperature of an ideal black body, emitting light with the same colour as the light source and measured in °K. In lighting industry, these temperatures are usually defined as "warm white","day white" etc. with actual values between about 2700 and 6500°K, the later been the most blue in colour. The obvious choice for ROV lights is the so called "cool white" LEDs with colour temperature between 5000 and 6500 °K. The colour temperature is not associated with a single wavelength λ but with rather a range of the spectrum - Fig. 6.3.
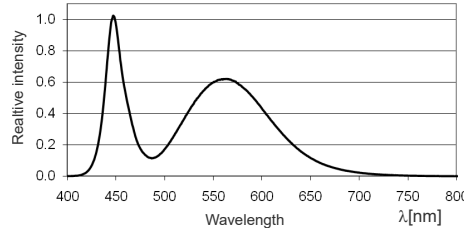

Fig. 6.3 Cool white LED spectrum.

The power can be calculated using Equation 6.4.
Example: What is the required lumen rating of a cool white LED light for a ROV, with the following requirements:

- d - operational distance to the object of interest - 3m.

- v, h - camera vertical and horizontal half angles - 30 and 60 degrees.

- C_{lx} - illuminance required by the camera - 100lx.

For the purpose of rough estimation, the average for a cool white LED $\lambda \approx 500$nm from Fig 6.3 can be used. The absorption coefficient for this λ is $\alpha(500) \approx 0.05$ m^{-1}. Substituting in Equation 6.4:

$$L_{lm}(0) \approx 100\pi 3^2 (\tan 30 + \tan 60)e^{0.05 \times 3} \tag{6.5}$$

$$L_{lm}(0) \approx 7580lm \tag{6.6}$$

Chapter 7:   Camera

In order to transmit a real-time video stream over an network channel, the bandwidth of the stream must be known. Obviously, the bandwidth is equal to the sensor resolution, multiplied by the pixel colour depth and the frame rate - Equation 7.1.

$$B_{vid}[\text{bps}] = R_i \times C_i \times C_d \times FR[\text{FPS}] \tag{7.1}$$

Where R_i and C_i are the image rows and columns, C_d is the colour depth and FR is the frame rate. Equation 7.1 allows bandwidth calculation of any raw image video stream. For example, a single image of a full HD frame is 1920x1080 pixels (in total it is about 2MP). The standard HD image contains 8 bit data per RGB channel, so the colour depth is 24 bit. With a frame rate of 30 FPS it is easy to calculate that the total bandwidth for a raw HD video stream is

$$B_{vid}[\text{bps}] = 1920 \times 1080 \times 24 \times 30\text{FPS} = 1500\text{Mpbs} \tag{7.2}$$

This is quite high bandwidth, not suitable for most network channels (keep in mind that still the most popular LAN is the 100 Mbps 100BASE Ethernet). The solution for this problem is compressing the still images, the video stream or both. There are several standard for video compression, most popular being MPEG1-4 and H.264. The compression standards and algorithms are not in the scope of this thesis, but it is worth mentioning that compressing the video stream reduces dramatically the required bandwidth. As mentioned in Chapter 3, a full HD1080p 30FPS surveillance camera produces no more than 7 Mbps video stream, which is more than 200 time less than the raw stream.

Chapter 8: Results and Conclusions

In the previous chapters, several novel approaches for solving various issues are proposed. In this chapter, all these approaches are put to test and the results are discussed and analysed. Further work is proposed where necessary.

8.1 Power

8.1.1 Prerequisites and setup

Several power related component have been chosen in order to comply with the high level requirements from Chapter 1:

- **Tether**. 500m cable with one PTP with wire cross section 2.5mm^2 each is ordered and supplied.

- **Power**. 2400W ROV power is specified. The selected PSU has a minimum operating voltage of 180V.

- **Voltage**. 220V standard European main grid voltage is used.

From these prerequisites the following parameters are devised:

- **Tether resistance** R_w. From equation 2.1

$$R_w[\Omega] \approx \frac{3.3 \times 10^{-2} \times 500\text{m}}{2.5[\text{mm}^2]} \tag{8.1}$$

$$R_w \approx 6.6\Omega \tag{8.2}$$

The real cable resistance is measured with an Ohmmeter and the result is 6.72Ω, which is very close to the theoretical one. The differences could be due to manufacturing tolerances. 6.72Ω are used for the further calculations.

- **Power**. 2400W ROV power is specified, with the selected PSU datasheet stating a minimum operating voltage of 180V. A quick check using Equation 2.2 -

$$P_{max}[\text{W}] \approx 7.62 \frac{2.5\text{mm}^2 \times 220\text{V}^2}{500\text{m}} \tag{8.3}$$

$$P_{max} \approx 1844\text{W} \tag{8.4}$$

This is much less than the required 2400W, so the only option is to increase the input voltage at the vessel. From the same Equation 2.2, the required input voltage is -

$$U_{in} \approx \sqrt{\frac{P_{max}l}{7.62A}} \tag{8.5}$$

and the calculated minimum voltage U_{in} is

$$U_{in}[\text{V}] \approx \sqrt{\frac{2400\text{W} \times 500\text{m}}{7.62 \times 2.5\text{mm}^2}} \tag{8.6}$$

$$U_{in} \approx 250\text{V} \tag{8.7}$$

The required voltage is achieved by a step-up transformer. Unfortunately, the voltage is very close to the maximum allowed voltage for the PSU (264V), so a voltage drop compensation is used as described in Chapters 2 and **??**.

The following schematic represent the power system test bench - Fig. 8.1.
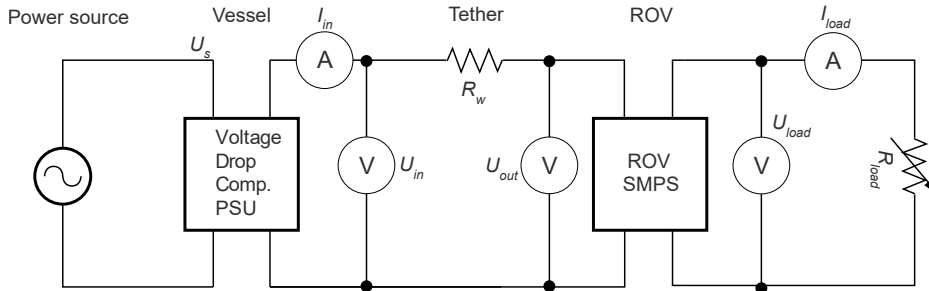
Fig. 8.1 Vessel and ROV power system test bench.

8.1.2 Methodology and results

The purpose of the experiment is to prove that in the range of the required power, the voltage at the ROV's PSU does not exceed the PSU maximum and minimum input voltages as stated in the data sheet. In the experiment the real tether is used with the measured resistance of $\approx 6.72\Omega$. A DC programmable load is used for the experiment. After powering the system, the load is gradually

increased from around 200W to 2400W. Five parameters are recorded - $U_{in}, I_w, U_{out}, U_{load}$ and I_{load}. From these, P_{in}, P_r and P_{load} are calculated. The results are presented in Table 8.1.

Table 8.1 ROV voltage vs ROV power.

Uin[V RMS]	Iin [A RMS]	Pin [W]	Pr[W]	Uout [V]	Uload [V]	Iload[A]	Pload[W]
238	1.01	240.4	232.3	210	15.79	12.54	197.92
238	1.98	471.2	443.5	204	15.76	23.95	377.47
238	3.1	737.8	672.7	197	15.78	36.27	572.40
238	4.05	963.9	850.5	190	15.83	45.71	723.60
238	4.98	1185.2	1015.9	184	15.81	54.73	865.00
238	6.03	1435.1	1187.9	180	15.72	64.25	1009.94
238	6.15	1463.7	1205.4	228	15.78	64.97	1024.90
282	5.45	1536.9	1335.3	225	15.71	72.25	1135.01
282	6.03	1700.5	1453.2	220	15.79	78.31	1236.70
282	6.98	1968.4	1640.3	211	15.77	88.48	1395.55
282	8.04	2267.3	1825.1	204	15.78	98.38	1552.69
282	8.8	2481.6	1953.6	198	15.71	105.73	1660.74

The most interesting column here is U_{out} which is the voltage applied to the ROV PSU. It is well in the range of accepted voltages as specified in the data sheet. The following chart shows the active voltage drop compensation - Fig. 8.2.
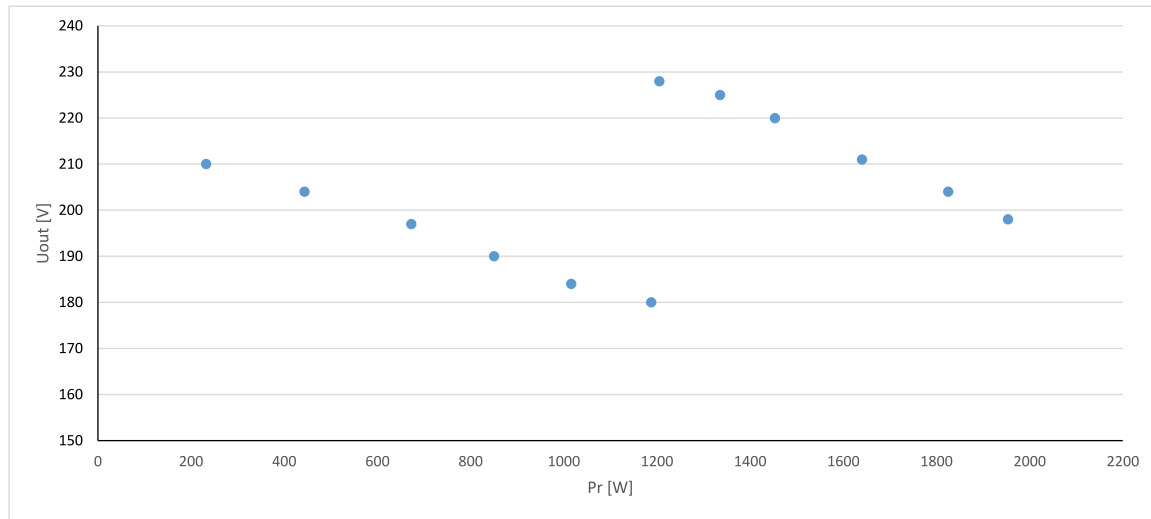

Fig. 8.2 Voltage drop compensation chart.

It is clearly visible that when the consumed power by the ROV reaches about 1200W, the PSU at the vessel switches to the next step-up voltage, in this case 282V. This results to an increase of about 45 volts at the ROV, which is still in the allowed range. The test has been performed over only one step-up threshold, due to the availability of the DC programmed load, which is rated to 2KW only. The algorithm performs perfectly and there is no doubt that it is going work over the full power range. No osculations have been observed. Az one disadvantage of the proposed solution can be mentioned the increased weight of the vessel PSU. The transformer must cover the ROV power requirements as

well as the losses in the tether. The transformer plus the control electronics weight is about 15kg, which is OK for large vessel but could be a problem for smaller boats. This is not an issue for a permanent ROV deployment vehicle, where the vessel PSU could be embedded in the on-board power system.

8.2   Camera

8.2.1   Setup

The chosen camera - Vivotek FD8169A - has an embedded video compression, but the bandwidth is not stated in the data sheet. The following setup has been arranged in order to test the camera bandwidth - Fig. 8.3.
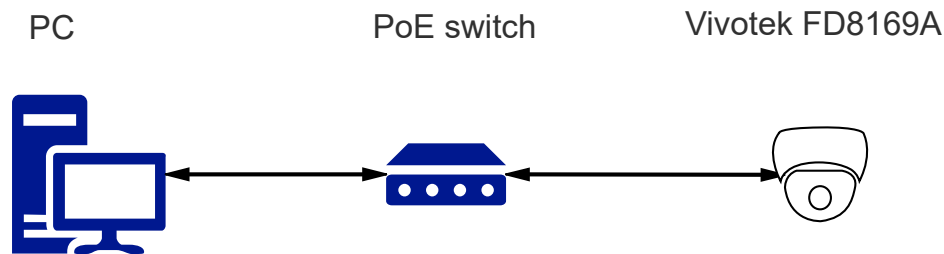

Fig. 8.3 Camera bandwidth measurement setup.

8.2.2   Methodology and results

The camera is set to it's higher resolution and frame rate - full HD 1080p, 30 fps. On the PC an IP traffic monitoring software is running. The software logs and shows the bandwidth used by all PC network connections. Two measurements are recorded, one with the camera plugged in the switch, one with the camera unplugged. The camera is pointed to a busy part of the room, with various colours and sharp edges which creates a maximum size images. Also, the camera is moved up and down constantly, using the servo, which changes the picture and making the compression more inefficient. This is the worst case scenario, usually much worse than a real underwater video material. The snapshot of the video on screen is shown on Fig. 8.4.

On the screen is shown some telemetry data also. Several scenes are tested, as well as different tilt camera speeds. As no difference is being observed, the following screenshots represent the results for any of the scenes and tilt speeds - Fig. 8.5, 8.6.

The traffic without the camera is negligible - around 10 Kbps. With the camera on it increases up to 3.3 Mbps. This is really low bandwidth camera as the expected traffic from Chapters 3 and 7 is between 5Mbps and 7Mbps. This makes probably all the comms requirements a bit of a overkill, but it is tested in the next section.
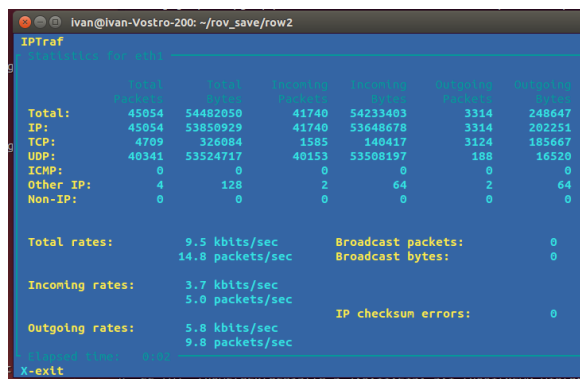
Fig. 8.4 Video stream snapshot.

Fig. 8.5 IP traffic monitor with the camera off.

8.3 Tether

The DC resistance, which is the main tether parameter affecting the power transfer is measured and taken into account in Section 8.1. For the purpose of transmitting data though, the impedance of the theter at higher frequencies must be measured and the characteristic impedance derived. This is necessary for getting the maximum throughput from the tether by terminating the PTP with appropriate value resistor.

8.3.1 Setup

The best way to measure the characteristic impedance of a transmission line is by using a Vector Network Analyser - VNA. Any network analyser measures the impedance and the return loss paramater S11. S11 is the difference, in decibels, between the amplitude of the incident wave and the reflected wave, so the goal is to get S11 as high as possible. The setup is presented on Fig. 8.7.
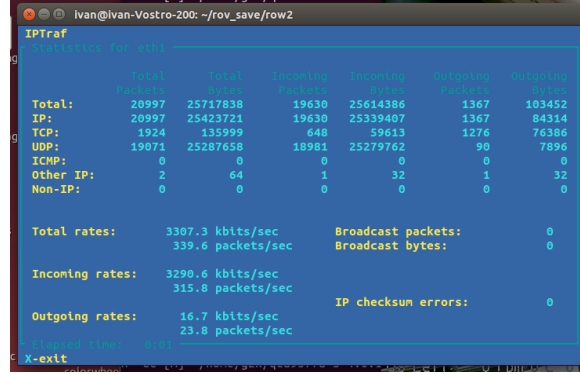
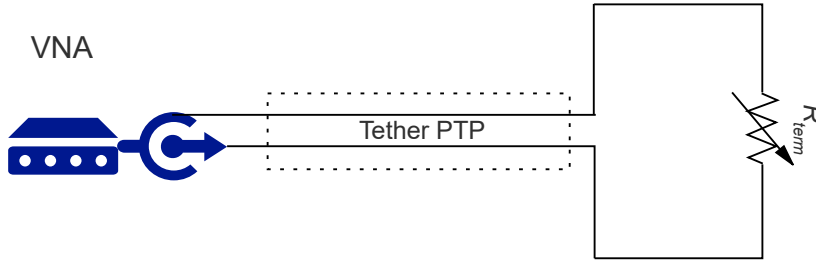Fig. 8.6 IP traffic monitor with the camera on.

Fig. 8.7 S11 parameter measurement setup.

8.3.2 Methodology and results

The S11 parameter has a maximum value when the line impedance matches the line termination resistor. The setup termination resistor R_{term} is a variable resistor of a maximum value of 100 Ohm. The VNA frequency range is set to be a bit larger tham the HomePlug required frequency range of 1.8 to 86.13 MHz, namely from 1 MHz to 100 MHz. Ten measurements are taken at 10 Ohm interval - from 10 Ohm to 100 Ohm. The S11 and the impedance are measured. The plots are superimposed on the same chart - Fig. 8.8.
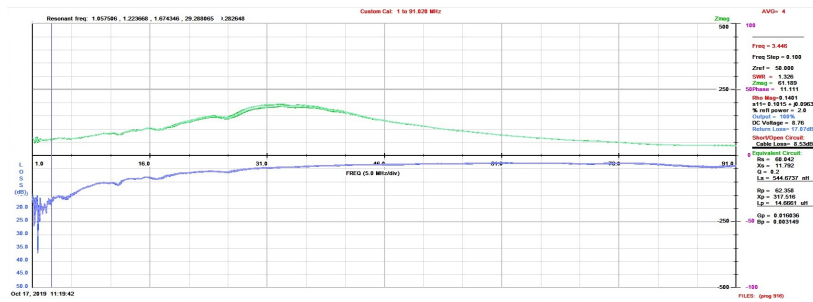

Fig. 8.8 S11 plots.

All plots are almost identical and overlapping, so there is no particular termination resistance that gives better results. S11 is quite low - around 3 to 5 dB in the largest part of the spectrum the HomePlug works in. This is definitely not an ideal transmission line, but an attempt is made in the

following section to measure the bandwidth and estimate if this line is good enough for carrying the video stream data. For comparison, another experiment is performed. In the place of the tether cable, a standard UTP cable is measured with a required terminating resistance od 100 Ohm. The plot is presented on Fig. 8.9.
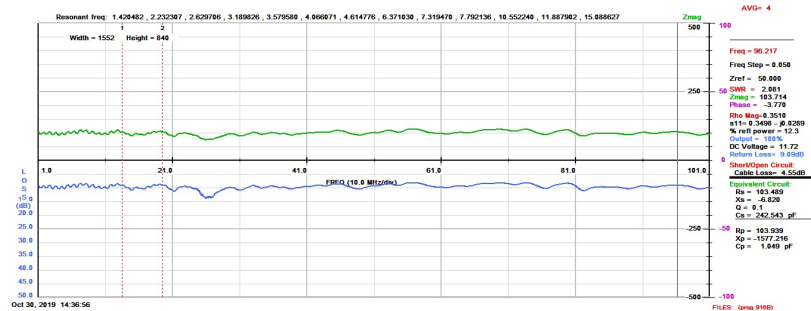
Fig. 8.9 S11 UTP plot.

The ideal transmission line has flat impedance plot, equal to the line characteristic impedance with S11 value equal to infinity. The UTP plot is not ideal, there are obvious losses, but it is much better than the tether, which is expected.

8.4 Comms

The main purpose of the comms test is to verify the assumption that the HomePlug technology provides enough bandwidth for the video stream. The second goal is to measure the lag between the RCC and the ROV which potentially could affect the ROV controllability.

8.4.1 Setup

One easy way to measure the network traffic and bandwidth is by usin an additional hardware device called network Terminal Access Point (TAP). The TAP device is a dedicated hardware, connected to the existing network with some administration software, allowing the operator to monitor the traffic an the network events remotely - Fig 8.10.

Fig. 8.10 Network Terminal Access Point (TAP).

As most of the TAPs provide the functionality to measure the bandwidth by default, no additional software tools are needed. Two TAPs are needed for channel bandwidth measurement as shown on Fig. 8.11. The administration monitoring software tool is running on a Windows OS based PC. UDP protocol is chosen randomly for tests as the high level protocol is irrelevant to the channel bandwidth. Four setups have been analysed, with the following channels -
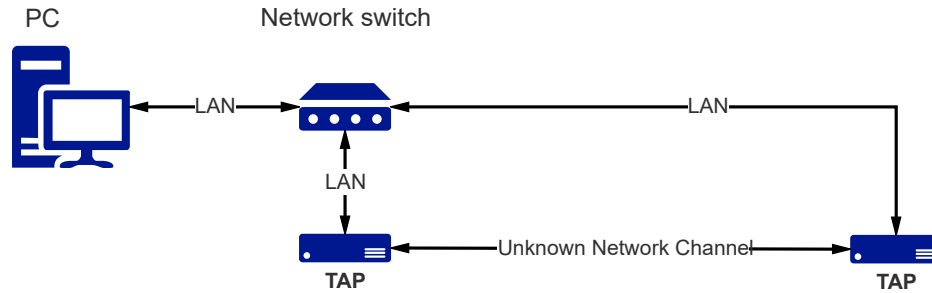
Fig. 8.11 Two TAPs setup.

- Direct LAN connection.

- HomePlug adapters connected on a same gang power socket.

- HomePlug adapters connected via 500m PTP (the ROV tether), no power load.

- HomePlug adapters connected via 500m PTP with 2KW power load.

8.4.2 Methodology and results

For each channel a Bandwidth Test from the monitoring software is performed - Fig. 8.12.
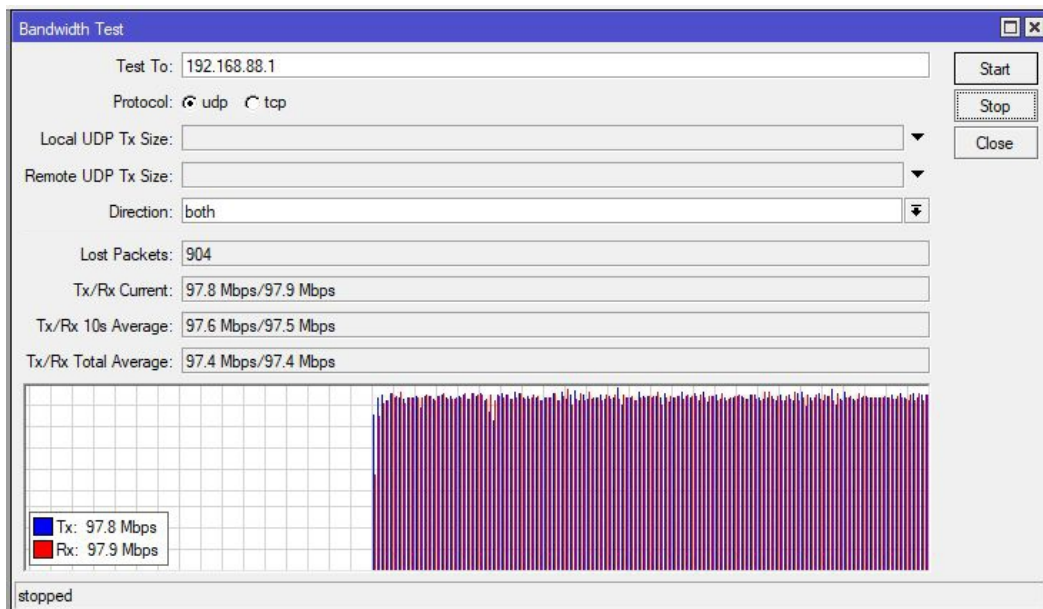
The test show the following results:

Fig. 8.12 TAP software bandwidth measurement.

- Direct LAN connection.

Fig. 8.13 LAN cable bandwidth measurement.

- HomePlug adapters connected on a same gang power socket.

Fig. 8.14 HomePlug short cable bandwidth measurement.

- HomePlug adapters connected via 500m PTP (the ROV tether), no power load.

Fig. 8.15 HomePlug long cable bandwidth measurement.
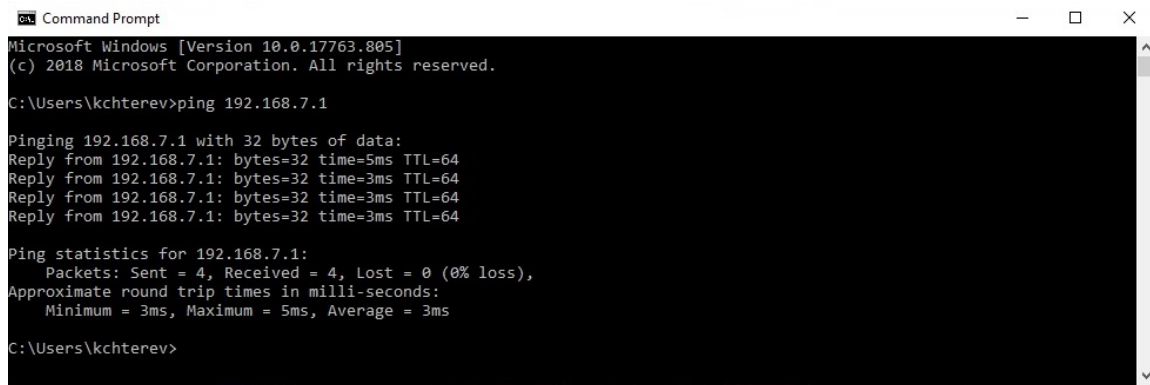
- HomePlug adapters connected via 500m PTP with 2KW power load.

Fig. 8.16 HomePlug long cable with load bandwidth measurement.

The direct LAN connection has obviously the highest throughput of about 100Mbps in both directions which is expected. The HomePlug adapters connected with a short cable perform reasonably well with $\approx$ 75Mbps in one direction and $\approx$35 Mbps in the other. The longer UTP obviously deteriorates the signal and the bandwidth drops significantly to $\approx$ 8.5 Mbps and $\approx$12 Mbps. Surprisingly, the same PTP with 2KW load performs much better, with $\approx$ 42 Mbps and $\approx$ 65 Mbps respectively. This is die to probably better transmission line matching. In worst case scenario, the minimum available bandwidth is greater than $\approx$ 8.5Mbps, which is more than twice than required by the chosen camera. The tests confirm that the HomePlug technology provides enough bandwidth over the 500m PTP for video streaming.

The second goal - network lag - is tested using the simple "ping" command which shows the time which the ping packet takes from the RCC to the ROV and back. A screenshot of the results is shown on Fig. 8.17

Fig. 8.17 HomePlug ping time measurement.

The ping time is 5ms maximum which is very low and would not affect the ROV controllability. As discussed in Chapter 3, in order the lag to have an effect on the ROV control, it must be more than 200ms. Both bandwidth and lag measurement test show the suitability of the HomePlug technology over long PTP for the main ROV high speed networking channel.

8.5 Thruster

Two goals are targeted regarding the ROV thruster. First - finding the best of selection of propeller and experimentally derive the thrust coefficient K_{th}. Second, using the derived K_{th}, resizing the test thruster to meet the required thrust. As mentioned in Chapter **??**, initially 60mm diameter propellers and Rice nozzle are manufactured. These are put to test together with some off-the-shelf products and compared.

8.5.1 Prerequisites and setup

A selection of propellers is either produced using 3D printing or purchased. Table 8.2 gives the propellers main characteristics.

Table 8.2 Propellers under test.

Propeller	Diameter [mm]	Blade number	EAR	P/D
Ka2-35-0.5-60	60	2	35	0.5
Ka2-35-0.6-60	60	2	35	0.6
Ka2-35-0.7-60	60	2	35	0.7
Ka3-52.5-0.5-60	60	3	52.5	0.5
Ka3-52.5-0.6-60	60	3	52.5	0.6
Ka3-52.5-0.7-60	60	3	52.5	0.7
Ka2-35-0.6-1.0-60	60	2	35	0.6-1.0
Ka2-35-1.0-60	60	2	35	1
Groupner 3-60	60	3	NA	NA
Groupner 2-60	60	2	NA	NA

The actual propellers are shown on Fig. 8.18.

Fig. 8.18 Selection of propeller to test.

The Rice nozzle with a holding bracket are 3D printed also. A small BLDC motor is selected for the tests - AX-2810Q, with a $K_v = 750$. The full propeller assembly is shown on Fig. 8.19.
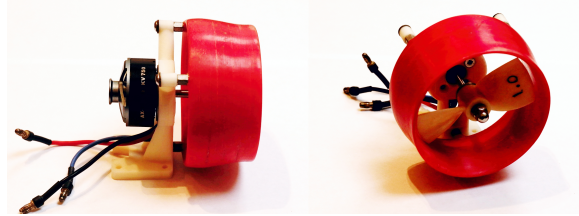
Fig. 8.19 Test thruster.

The test are performed in a pool, with a setup as drawn on Fig. 8.20.

The test thruster is attached to a swinging arm, which can rotate around a pivot axis. The thrust is measured by a dynamometer attached on equal distance from the pivot axis to the propeller rotation axis. This way, the force measured by the dynamometer is exactly equal to the thrust produced. The supplied voltage is decided to be 11.1V, which produces a maximum of $11.1\text{V} \times 750\text{RPM/V} = 8325\text{RPM}$.

8.5.2 Methodology and results

The first goal to be targeted is to find the "best" of the selected propellers. For each propeller several measurements are performed, recording the rotational speed f_t, consumed current I_t and produced thrust F_t. The criterion for selection is obvious - the thruster which produces more Bollard thrust per unit of electrical power is the best. The measurement procedure is simple. The ESC is controlled to produce predefined RPMs, at which the current and the thrust are recorded. The results are presented in Tables 8.3, 8.4 and 8.5.

The data is plotted on a thrust vs. current graph - Fig. 8.21. For simplicity, the current is used instead of power, as the voltage is a constant.
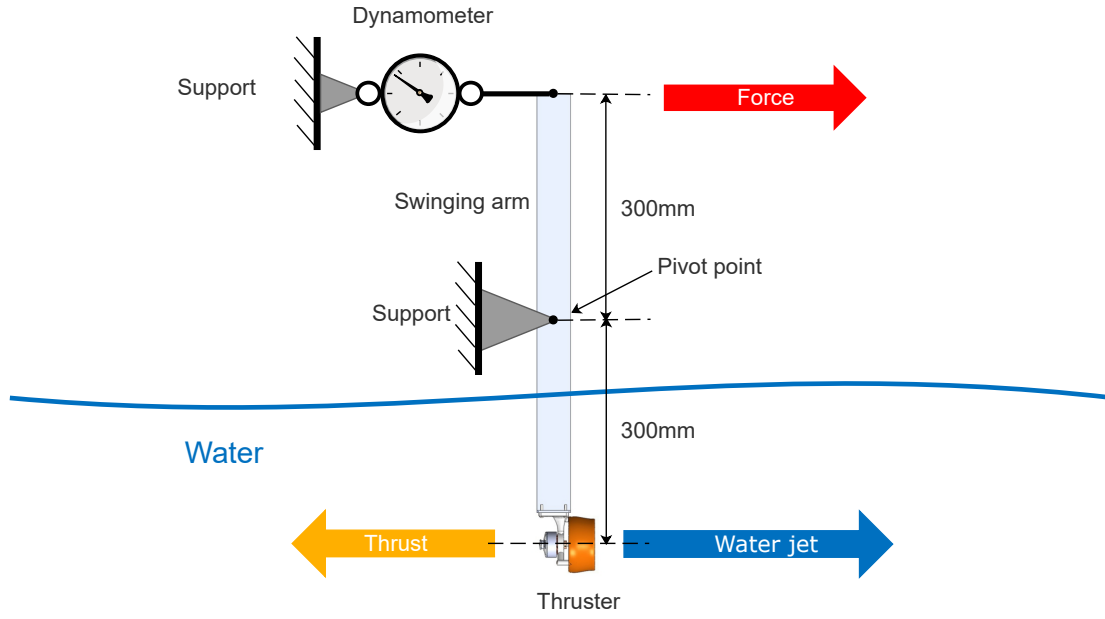
Fig. 8.20 Test setup.

Table 8.3 Propellers thrust vs. electrical power data.

ft		Propeller: Ka2-35- 0.5 - 60 Voltage: 11.1			Propeller: Ka2 -35- 0.6 - 60 Voltage: 11.1			Propeller: Ka2 -35- 0.7 - 60 Voltage: 11.1		
Hz	RPM	I [A]	F [kg]	P [W]	I [A]	F [kg]	P [W]	I [A]	F [kg]	P [W]
58	500	0.17	0	1.887	0.16	0	1.776	0.16	0	1.776
116	1000	0.27	0	2.997	0.24	0.05	2.664	0.25	0.05	2.775
175	1500	0.41	0.08	4.551	0.45	0.12	4.995	0.46	0.13	5.106
233	2000	0.69	0.16	7.659	0.82	0.26	9.102	0.85	0.27	9.435
291	2500	1.07	0.25	11.877	1.4	0.4	15.54	1.6	0.47	17.76
350	3000	1.65	0.37	18.315	2.25	0.6	24.975	2.45	0.67	27.195
408	3500	2.6	0.54	28.86	3.25	0.85	36.075	3.9	0.93	43.29
466	4000	3.3	0.73	36.63	4.6	1.1	51.06	5.6	1.3	62.16
525	4500	4.6	0.9	51.06	6.4	1.4	71.04	8	1.6	88.8
583	5000	6.4	1.15	71.04	8.4	1.8	93.24	10.2	2.1	113.22
641	5500	8.1	1.35	89.91	11.2	2.3	124.32	13.5	2.7	149.85
700	6000	10.25	1.6	113.775	14.4	2.7	159.84	16	3.1	177.6
758	6500	12.5	1.7							

There are two clear winners according to the graph - Ka2-35-0.6-1.0-60 and Ka2-35-1.0-60. Ka2-35-1.0-60 is chosen due to it's simpler design.

The second goal is to find the thruster thrust coefficient K_{th}. Equation 8.18 can be rewritten as

$$F_t = K_{th0} \times f_t^2 \tag{8.8}$$

where

$$K_{th0} = K_{th} \times \rho_w \times D^4 \tag{8.9}$$

Table 8.4 Propellers thrust vs. electrical power data.

ft		Propeller: Ka3-52.5 - 0.5 - 60 Voltage: 11.1 V			Propeller: Ka3-52.5 - 0.6 - 60 Voltage: 11.1 V			Propeller: Ka3 -52.5- 0.7 - 60 Voltage: 11.1 V		
Hz	RPM	I [A]	F [kg]	P [W]	I [A]	F [kg]	P [W]	I [A]	F [kg]	P [W]
58	500	0.16	0	1.776	0.13	0	1.443	0.16	0	1.776
116	1000	0.21	0	2.331	0.22	0.05	2.442	0.25	0.07	2.775
175	1500	0.41	0.08	4.551	0.45	0.13	4.995	0.51	0.16	5.661
233	2000	0.78	0.18	8.658	0.79	0.23	8.769	0.92	0.31	10.212
291	2500	1.24	0.25	13.764	1.39	0.38	15.429	1.75	0.52	19.425
350	3000	2.08	0.33	23.088	2.15	0.5	23.865	2.7	0.75	29.97
408	3500	3.1	0.5	34.41	3.25	0.8	36.075	4	1	44.4
466	4000	4.45	0.7	49.395	4.5	1	49.95	6.2	1.4	68.82
525	4500	6.35	0.8	70.485	7.5	1.25	83.25	8.5	1.8	94.35
583	5000	9	0.95	99.9	10.3	1.55	114.33	11.5	2.25	127.65
641	5500	12.2	1.05	135.42	12.7	1.94	140.97	14	2.65	155.4
700	6000	15.9	1.08	176.49	15.3	2.13	169.83	17	2.9	188.7
758	6500									

Table 8.5 Propellers thrust vs. electrical power data.

ft		Propeller: Groupner 3-60 Voltage: 11.1 V			Propeller: Groupner 2-60 Voltage: 11.1 V			Propeller: Ka2-35-0.6-1.0-60 Voltage: 11.1 V			Propeller: K2-35-1.0-60 Voltage: 11.1 V		
Hz	RPM	I [A]	F [kg]	P [W]	I [A]	F [kg]	P [W]	I [A]	F [kg]	P [W]	I [A]	F [kg]	P [W]
58	500	0.16	0	1.776	0.14	0	1.554	0.19	0	2.109	0.19	0	2.109
116	1000	0.23	0.05	2.553	0.24	0.06	2.664	0.31	0.08	3.441	0.31	0.12	3.441
175	1500	0.46	0.12	5.106	0.44	0.13	4.884	0.69	0.25	7.659	0.74	0.28	8.214
233	2000	0.84	0.24	9.324	0.85	0.25	9.435	1.3	0.49	14.43	1.4	0.51	15.54
291	2500	1.34	0.4	14.874	1.35	0.4	14.985	2.45	0.8	27.195	2.45	0.81	27.195
350	3000	2.2	0.57	24.42	2.3	0.6	25.53	4	1.15	44.4	3.95	1.2	43.845
408	3500	3.25	0.72	36.075	3.25	0.82	36.075	6	1.5	66.6	6	1.65	66.6
466	4000	4.7	1.1	52.17	5	1.15	55.5	9	2.09	99.9	9	2.05	99.9
525	4500	6.4	1.35	71.04	6.6	1.5	73.26	13	2.79	144.3	12.5	2.65	138.75
583	5000	9	1.65	99.9	8.7	1.7	96.57	16	3	177.6	17.2	3.25	190.92
641	5500	11.2	2	124.32	12.2	2.2	135.42						
700	6000	14	2.35	155.4	15.5	2.5	172.05						
758	6500												

From Table 8.5 a plot can be constructed showing the quadratic relationship between F_t and f_t - Fig. 8.22.

The graph clearly shows quadratic relationship and the trendline equation is

$$F_t \approx 0.0046 f_t^2 \ , \ K_{th0} \approx 0.0046 \tag{8.10}$$

The linear member is ignored as the coefficient in front is far too small. Now K_{th} can be calculated

$$K_{th} = \frac{K_{th0}}{\rho_w \times D^4} \tag{8.11}$$

$$K_{th} \approx \frac{0.0046}{1000 \times 0.06^4} \tag{8.12}$$
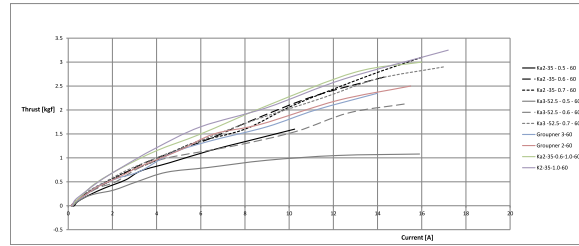
Fig. 8.21 Propellers thrust vs. current graph.
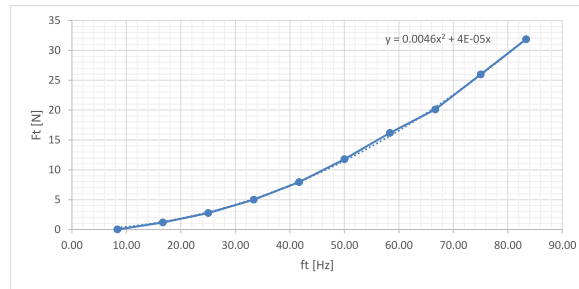
Fig. 8.22 Propeller thrust vs. frequency graph.

$$K_{th} \approx 0.35 \tag{8.13}$$

Using the calculated K_{th} the second goal - resizing the thruster, can be achieved. The total thrust is set to 50 kgf. It must be delivered by 4 horizontal thrusters in a vector formation - Fig. 8.23
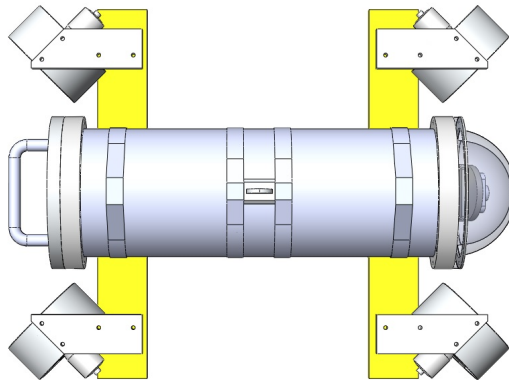
Fig. 8.23 Vectored thruster formation.

All 4 horizontal thrusters are at 45 degrees relative to the ROV X and Y axes. This way, the operator has full control of the ROV in XY plane - translational and rotational. The disadvantage of this configuration is that in any direction, the maximum thrust that can be achieved is the total thrust of all thrusters multiplied by $cos(\pi/4) \approx 0.7$, so about 30% of the thrust is lost. The advantages of

having full control are more attractive though, so a compromise is made. From here, the maximum thrust for an individual thruster can be found:

$$F_{tot} = N_t \times F_t \times cos(\pi/4) \tag{8.14}$$

Where F_{tot} is the tothal ROV thrust, F_t is the thrust of an individual thruster and N_t is the number of thrusters. The individual thrust required is

$$F_t = \frac{F_{tot}}{N_t \times cos(\pi/4)} \tag{8.15}$$

Substituting with the real numbers

$$F_t = \frac{50\text{kgf}}{4 \times cos(\pi/4)} \tag{8.16}$$

or

$$F_t \approx 17.7\text{kgf} \approx 173.4\text{N} \tag{8.17}$$

per thruster. the Kaplan Bollard thrust is

$$F_t = K_{th} \times \rho_w \times D^4 \times f_t^2 \tag{8.18}$$

where $K_{th} \approx .35$ is a thrust coefficient, measured in Chapter 8, $\rho_w \approx 1000\text{Kg/m}^3$ is the water density and f_t is the rotational frequency of the propeller. We selected the motor with maximum power output around 2500 RPM, or 42Hz, so the required propeller diameter can be calculated:

$$D = \sqrt[4]{\frac{F_t}{K_{th} \times \rho_w \times f_t^2}} \tag{8.19}$$

$$D \approx \sqrt[4]{\frac{173.4\text{N}}{0.35 \times 1000\text{Kg/m}^3 \times 42^2\text{Hz}}} \tag{8.20}$$

$$D \approx 0.129\text{m} \tag{8.21}$$

With some considerations that this is an ideal case, a bit of reserve is needed, so the selected diameter is $D = 0.135$m.

One more check is required and this is the propeller power at the maximum thrust. This is needed to verify that the available electrical power from the main PSU is enough to supply the thrusters. The equation for an ideal propeller used is -

$$F_t^{1.5} = W_p\sqrt{2\rho A_p} \tag{8.22}$$

Where W_p is the total input power, ρ s the water density and A_p is the propeller area. From here

$$W_p = \frac{F_t^{1.5}}{\sqrt{2\rho A_p}} \tag{8.23}$$

$$W_p = \frac{F_t^{1.5}}{\sqrt{2\rho\pi R^2}} \tag{8.24}$$

$$W_p[\text{W}] \approx \frac{173.4[\text{N}]^{1.5}}{\sqrt{2 \times 1000[\text{kg/m}^3] \times \pi \times 0.0675[\text{m}]^2}} \tag{8.25}$$

$$W_p \approx 426.7[\text{W}] \tag{8.26}$$

W_p is the total input power, which can be translated to electrical power P_{rov} using

$$P_{rov} = \frac{N_t \times W_p}{\eta_p\eta_m} \tag{8.27}$$

where η_p and η_m are the efficiencies of the PSU and the BLDC motor. From these, the PSU efficiency is known from the datasheet - $\eta_p = 89\%$. The BLDC motor efficiency is assumed to be around 90%. The electrical power supplied to the ROV is

$$P_{rov}[\text{W}] = \frac{4 \times 426.7\text{W}}{89\% \times 90\%} \tag{8.28}$$

$$P_{rov} \approx 2130.8\text{W} \tag{8.29}$$

The P_{rov} is less than the available power of 2400W as stated in Section 8.1, so the goal for 50kgf total thrust set in Chapter 1 can be achieved with the proposed configuration.

8.6   Lights

The graph on the Fig 6.2 shows that in general, a light with a wavelength towards the blue region of the spectrum penetrates better than any other wavelengths. Thus, a cool white LEDs are decided to be used for the project. In this section, three different colour temperature LEDs are put to test and analysed for performance. The obvious criterion is the minimal light power loss in water, comparing to air. The test is qualitative, as no high precision photometric equipment is available at the time.

8.6.1   Setup

The setup consists of an off-the-shelf digital camera, black PVC tube with transparent caps on both sides, opal acrylic screen, bench power supply and a LED board containing the tree LEDs under test . The arrangement is shown on Fig. 8.24.
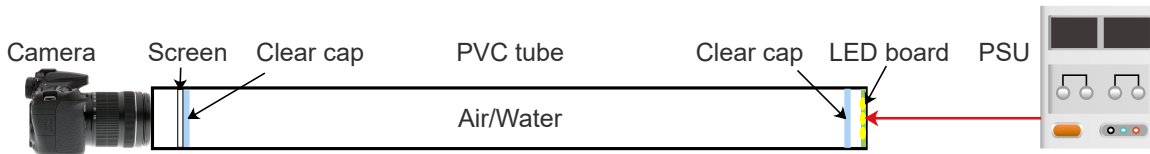

Fig. 8.24 LED performance setup.

The PVC tube is watertight and can be filled with water. Fresh water from the tap is used for the experiment. The camera and the LED board are optically shielded so, no ambient light can penetrate inside of the tube. The camera is set to manual mode, with aperture number 8, shutter speed 1/60 sec, colour balance - RAW (uncorrected), ISO 400. The lens focal length is 35mm (50mm equivalent of 35mm film camera) focus set to infinity. The three LEDs are made by CREE with the following characteristics -

- PN-CXA1507-0000-000N00G430G, Warm White, 14.8W, 840lm, 200mA,3000^0K

- PN-CXA1507-0000-000N0HG440G, Neutral White, 14.8W, 840lm, 200mA, 4000^0K

- PN-CXA1507-0000-000N0HG450G, Cool White, 14.8W, 840lm, 200mA, 5000^0K

8.6.2   Methodology and results

The goal is to measure the opal screen illuminance with each of the LEDs individually powered. The bench PSU is set to 36.35V DC with a LED current consumption at this voltage of 220mA. Three pictures with no water in the PVC tube are taken all three LEDs. The test is repeated with the tube filled with tap water. The images taken are presented in Figs. 8.25 and 8.26.
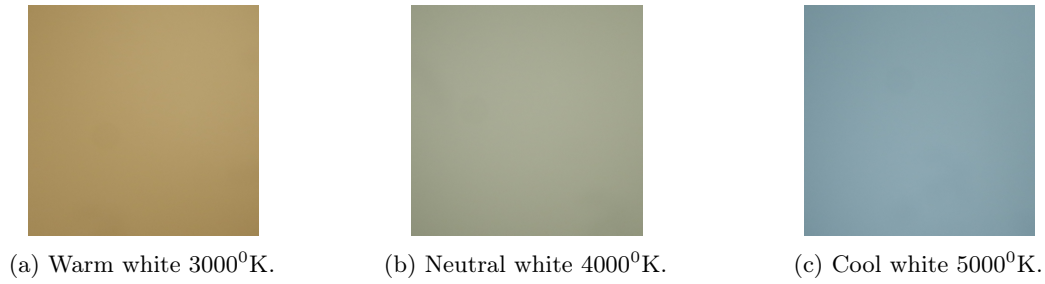
(a) Warm white 3000^0K.   (b) Neutral white 4000^0K.   (c) Cool white 5000^0K.

Fig. 8.25 LED images with no water filled tube.

(a) Warm white 3000^0K.   (b) Neutral white 4000^0K.   (c) Cool white 5000^0K.
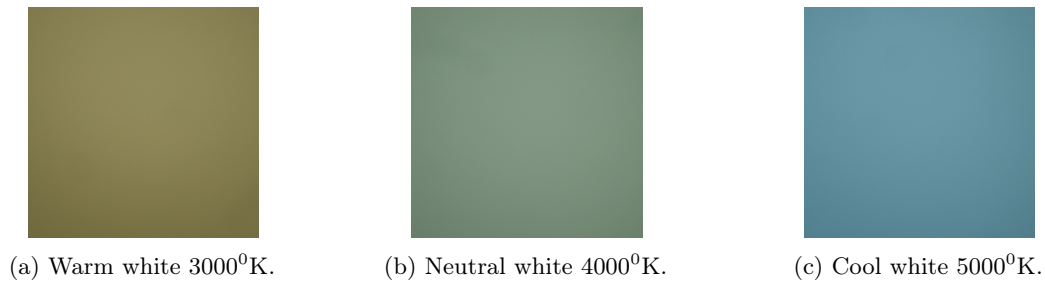
Fig. 8.26 LED images with tap water filled tube.

There is obviously reduction of the light intensity when the tube is filled with water due to absorption mainly. For each image an average of all three RGB channels is taken. The illiuminance is recorded as a sum of the RGB channels values. The result are shown in Table 8.6.

Table 8.6 LED Screen illuminance measurement.

	3000K-air	4000K-air	5000K-air	3000K-water	4000K-water	5000K-water
R	176	161	133	134	123	98
G	150	165	160	122	142	146
B	95	143	170	76	122	161
Total illum.	421	469	463	332	387	405
Total loss				89	82	58

This method of illuminance measurement cannot provide absolute values, but can be used for comparative qualitative analysis. The first observation is that the 4000^0K and the 5000^0K LEDs are performing similarly in air, while the 3000^0K one despite having an equal intensity, provide much less illuminance. The most important result though is the total loss measurement, which is the difference between the measurements in air and in water. Here, the 5000^0K cool white LED is clear winner with a total loss of 58 illuminance units vs. 82 for the 4000^0K one. Just for quick validation, the Equation 6.3 is used to derive the theoretical transmitted light intensity $L_{lm}(d)$ per each RGB channel. The distance d is 1.0m and the absorption coefficient is taken roughly from the graph on the Fig. 6.2. The results are presented in Table 8.7.

The theoretical results are close to the measured values, with differences that can be accounted to measurement errors and the difference between chosen RGB wavelengths which are unknown for the camera sensor.

Table 8.7 LED transmitted intensity $L_{lm}(1)$ calculation.

	α(λ)[m-1]	3000K-water	4000K-water	5000K-water
R - Llm 640nm	0.35	124	113	94
G - Llm 580nm	0.15	129	142	138
B - Llm 460nm	0.01	94	142	168

8.7   Conclusions

The high level requirements for the project are set in Chapter 1. First, the product capabilities are tested in one expedition organised by the Institute of Oceanology - Varna in the autumn of 2016. The ROV was deployed from the RV Akademik at 70m depth. The apparatus showed good controllability and video stream quality. Some still images are shown on Fig. 8.27.
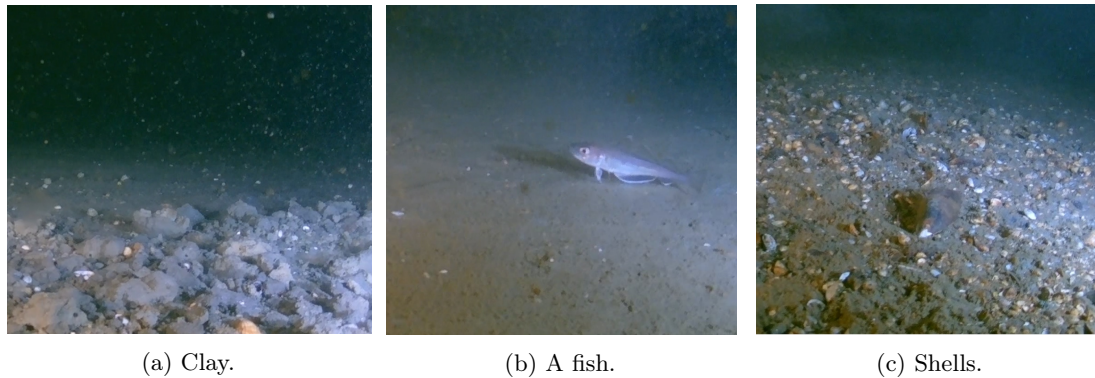

(a) Clay.   (b) A fish.   (c) Shells.

Fig. 8.27 Black Sea shelf images taken by the ROV.

Links to the full length videos from the expedition can be found in Appendix **??**. The major work on the ROV has been completed during 2013-2016, but is still in progress and the versions of the hardware and software are constantly upgraded. It is safe to say though, that the ROV has been completed in 3 years time, complying with the requirement. Calculating the budges is not so easy as many components are either manufactured in house or provided for free from third parties. The following table makes the best estimate of the project cost - Table 8.8. As shown, the total manufacturing cost of about $13 000, including the R&D for some components, is far less than the originally assigned budget of $20 000. In the next subsections, the results of all the ROV components are reviewed.

8.7.1   Power

The ROV power architecture is based on a voltage drop compensated vessel PSU. The goal of compensating the voltage reaching the ROV is achieved by stepping-up the vessel PSU voltage depending on the consumed power by the ROV. The system is stable and the method can be used for any ROV or similar long wire problem projects. One disadvantage is the higher cost and weight of the vessel equipment. Also, as the continental shelf is only at about 100-120m depth, if a shorter

Table 8.8 Sea Turtle II project cost estimation.

Item	BOM price [USD]	Labour price [USD]	Qty.	Total [USD]
Power				
RCC PSU	250	0	1	250
15V 2.4KW PSU	1500	0	1	1500
38V PSU	65	0	1	65
PoE Injector	75	0	1	75
PSU filter	15	20	2	70
				0
Comms				0
HomePlugs	150	0	1	150
LAN-to-LIN	20	0	1	20
				0
Tehter				0
Cable	5.5	0	500	2750
Reel	120	250	1	370
Mercotac conector	85	0	1	85
WetCon connector	120	0	1	120
				0
Thruster				0
Nozzle	25	35	6	360
Propeller	15	35	6	300
Motor	65	20	6	510
Controller	35	50	6	510
Controller R&D	0	1200	1	1200
Lights				
LED	7	0	4	28
Holder	3	10	4	52
				0
Mechanics				0
Pressure tube	125	350	1	475
Illuminator	135	0	1	135
Steel frame	55	300	1	355
Float	65	250	1	315
				0
Other				0
Wires	60	0	1	60
I/O Board R&D	0	700	1	700
I/O Board	30	0	1	30
Seals and gaskets	20	0	2	40
Connectors	1	0	50	50
RCC computer	1200	0	1	1200
RCC enclosure	50	0	1	50
Final assembly	0	1000	1	1000
Total				12825

tether is used, the voltage drop is negligible and no compensation is needed. If implemented though, even at shorter distances a thinner tether can be used, minimising the overall weight and drag, so still the method is an useful option when transferring power over long cables. With low voltage motors though, the PSU in the ROV is inevitably large, expensive and heavy, which is one of the limitations of the method.

8.7.2 Tether and Communications

One of the important results of this work is the proof that a single pair power cable can be used for both transferring power and communications. the PTP is extremely easy to work with, cheap and

available from any cable manufacturers. A 2.5 mm^2 PTP tether can provide up to 2500KW over 500m distance and 13 Mbps bandwidth for comms, which is plenty for most ROV applications. The PTP S11 plot - Fig. 8.8 - reveals that even there is no clear characteristic impedance, the HomePlug technology can be successfully used for extending the LAN over a long cable with a reasonable bandwidth and response time. The LUNA proved to be working fine, minimising the cost and wire counts in the ROV.

8.7.3 Thruster

Two of the main thruster components - the propeller and the controller have been designed from scratch and proved to be providing the required thrust as stated in Chapter 1. One of the important outcomes is the 2 blade Kaplan propeller. Its performance is superior to the other propellers and has never been seen implemented on other ROVs. The thrust coefficient K_{th} of such propeller is small - about 0.35, which is crucial when high RPM motors are used. These motors are usually designed for model cars, planes and drones, where obviously high K_v is required. The lower K_{th} compensates the high K_v and makes possible the low cost BLDCs to be used in ROV applications.

8.7.4 Lights

As the waters absorbs more the red part of the light spectrum, it is obvious that if more energy is emitted in the blue region, more efficient the light source is under water. Most power LEDs have a complex spectrum though, so it is not clear how the LED colour temperature affect the LED light penetration in water. The test proved the expectation that the cool white LED - 5000^0K performs significantly better than the lower colour temperature ones. The efficiency gain is more than 25% which is not an issue in the current project, but is important in a battery operated small ROVs, where the thruster power is comparable with the lights.

8.7.5 Camera

The camera choice for underwater application is between an analogue type, which require a dedicated analogue channel in the tether, or a digital camera, with a network interface. The obvious choice is the second one, due to the decision to have a single PTP tether. The selected camera is not of the highest end of products, but performs adequately and provides little lag. The bandwidth is small and well in the range of the HomePlug over PTP.